Spectroscopic Confirmation of Four Ultra Diffuse Galaxy Candidates in Group Environments

Research Thesis

Presented in partial fulfillment of the requirements for graduation *with research distinction* in Astronomy and Astrophysics in the undergraduate colleges of The Ohio State University

by

Conor Hayes

The Ohio State University

May 2020

Project Advisors: Dr. Paul Martini, Dr. Johnny Greco

Abstract

Ultra diffuse galaxies (UDGs) are a type of low surface brightness galaxy that have garnered much interest in the astronomical community in recent years in part because their high dark to baryonic matter ratios make them ideal testing grounds for the assumptions of the ΛCDM cosmological framework. Measuring redshifts of these objects is of critical importance because it allows us to understand their physical properties and, through comparisons with established galaxy catalogues, the environments in which they live. In this work, I present redshift measurements for four UDG candidates. Through these measurements, I have determined that these objects exist in group environments. Because the number of UDGs in similar environments with confirmed distances is presently quite small, this represents an important addition to our catalogues of the low surface brightness universe.

Contents

Chapter 1

Introduction

Over a period of ten days in December 1995, the Hubble Space Telescope stared at a relatively unexciting patch of the sky about 2.6 arcminutes across. The resulting image, now known as the Hubble Deep Field, revealed a universe packed full of galaxies. Despite covering only one 24-millionth of the sky, the HDF contained roughly 3,000 galaxies and became a foundational data set for astronomers studying the early universe. However, small, deep-field images like the HDF can't tell the whole story about how galaxies form. The need for a wide-field imaging survey was the primary motivation behind the project that eventually became the Sloan Digital Sky Survey (SDSS; York et al., 2000). While SDSS quickly became the most prolific extragalactic survey to date, it, like nearly all ground-based surveys, is biased towards the high surface brightness universe. This is thanks in part to the fact that the night sky, even under the most optimal of observing conditions, is not perfectly dark. Due to a multitude of factors, the sky has a minimum intrinsic surface brightness of $\sim 22 - 23$ mag arcsec^{-2} (Leinert et al., 1998). As a consequence, any objects with a surface brightness less than this can be extremely difficult to detect from ground-based telescopes.

For many decades, it was unclear if low surface brightness objects even existed. Glimmers of a potential problem emerged in Freeman (1970), where an analysis of thirty-six disk galaxies revealed that twenty-eight had average surface brightnesses in the very narrow range of 21.65 ± 0.3 mag arcsec $^{-1}$, despite the fact that their absolute magnitudes varied by nearly

5 mag. Seizing on the fact that this value was suspiciously close to the average sky brightness, Disney (1976) argued that low surface brightness galaxies (LSBGs) might be systematically underrepresented in galaxy population analyses. Indeed, it is now believed that LSBGs make up a large fraction of the total number of galaxies in our universe (e.g. Impey & Bothun, 1997). If we wish to accurately understand the nature of the universe through observations of galaxies, it is critically important that we accurately understand the nature of LSBGs.

Due to the detection difficulties created by the sky brightness problem, data concerning LSBGs have been severely limited until quite recently. While one might think that we would be able to use space telescopes to circumvent the issues inherent to living on a planet with an atmosphere, it turns out that they aren't all that useful to low surface brightness astronomy. Firstly, they are quite expensive to launch and maintain. This has the consequence of limiting the amount of time that they can dedicate to any one project, meaning that reaching the exposure times required to obtain useful imaging data for LSBGs is quite difficult. Furthermore, they are subject to the same systematic errors as all reflecting telescopes, primarily diffraction and scattered light from the telescope assembly, which contaminate images below ~ 29 mag arcsec $^{-1}$ (Abraham & van Dokkum, 2014). This difficulty is further compounded by the fact that to obtain a statistically significant sample of LSBGs, we will need deep field surveys that can image a large portion of the sky, rather than just a tiny fraction of it. SDSS has been of some help, but even its utility to LSBG studies has been inhibited by its surface brightness limits.

Fortunately, not all is lost. Recent years have seen the development and implementation of the next generation of wide-field imaging surveys. These surveys, including the Dark Energy Survey (DES; Dark Energy Survey Collaboration et al., 2016), the Kilo-Degree Survey (KiDS; de Jong et al., 2015), the Hyper Surprime-Cam Subaru Strategic Program (HSC-SSP Miyazaki et al., 2018), and the upcoming Vera C. Rubin Observatory (Ivezic et al., 2008), will allow us to probe the universe at ever-lower surface brightnesses. Several examples of the advantages that these surveys provide us over longer-standing surveys like SDSS are

presented in Figure 1.1. Despite these advances, our knowledge of the general properties of LSBGs is still severely lacking, particularly at low stellar masses. What we do know is that they are incredibly varied across all galaxy properties and that the limits of this variability have not yet been rigorously tested for a statistically significant sample (though efforts were made to do so in the 90s, e.g. Dalcanton et al., 1997a; McGaugh & Bothun, 1994; McGaugh, 1994; McGaugh et al., 1995), creating an urgent need to identify and study these objects.

A subcategory of LSBGs that has generated a great deal of interest in recent years are so-called "Ultra Diffuse Galaxies", or UDGs. While the definition of what exactly constitutes a UDG is variable across the literature, they are generally characterized as being physically quite large with very small stellar masses, often spreading a dwarf galaxy's mass ($\sim 10^7 - 10^9 M_\odot$) over an area the size of the Milky Way ($r_{eff} \sim 1.5 - 5$ kpc). This results in central surface brightnesses between 25 and 27 mag arcsec $^{-1}$. While the first UDG was discovered in 1984 (Sandage & Binggeli, 1984), it was not until 2015 when the Dragonfly Telephoto Array discovered 47 UDGs in the Coma Cluster (van Dokkum et al., 2015) that interest in these objects really picked up. Indeed, the discovery of these UDGs reignited the astronomical community's interest in LSBGs in general. The mechanisms behind the formation of objects like these are still an area of active research, but essentially three models have emerged:

1. UDGs live in the "high spin tail" of the galactic spin rate distribution. They formed in dark matter halos with higher than average angular momentum, resulting in their larger radii. (e.g. Dalcanton et al., 1997b; Amorisco & Loeb, 2016)

2. UDGs are the result of dwarfs with a bursty star formation history, where stellar feedback mechanisms gradually pushed the entire stellar population outward. (e.g. El-Badry et al., 2016; Di Cintio et al., 2017)

3. UDGs are "failed" L*-scale galaxies that had their gas stripped by environmental effects after forming their first generation of stars. (e.g. van Dokkum et al., 2015)

Determining which of these (if any) is the dominating process in UDG formation is a

complex problem. Most UDGs have been found in cluster environments, where it can be difficult to discern between features that are the result of formational processes and those that are the result of environmental interactions. As a consequence, we are interested in studying isolated UDGs, as their evolution has not been influenced by massive neighbors.

In general, UDGs that have been discovered thus far have tended to follow the characteristic morphology-density relation seen across the galactic population in general. Those in clusters are red and quenched, while those in the field are blue and star-forming. If we can find a population of quenched UDGs outside of cluster environments, then that could suggest that cluster UDGs were not quenched by their environment, as has traditionally been believed. Instead, their physical properties would be the result of internal mechanisms inherent to their formation.

Previous studies (e.g. Geha et al. (2012)) have determined that quenched dwarf galaxies below a stellar mass of $10^9 M_\odot$ are extremely rare in the field, and this is consistent with the fact that UDGs discovered in the field have been blue and star-forming (Leisman et al., 2017). However, these results may be biased by the fact that these isolated UDGs were identified through their HI content, and quenched galaxies would be deficient in HI. This is part of what makes optical surveys like HSC-SSP so powerful. Because they are sensitive to the starlight of LSBGs, they can detect these objects regardless of their gas fraction (down to the survey's surface brightness sensitivity). As such, if quenched UDGs exist in the field, HSC-SSP and similar surveys should be able to find them.

Studies of LSBGs, and UDGs in particular, are also important testing grounds for cosmological models. While the dominant ΛCDM model does an excellent job of predicting the large-scale structures of the universe, smaller-scale simulations have encountered a number of serious problems. Among these are the "missing satellites problem", wherein simulations of Milky Way-like halos produce far more dwarf satellites than we see in observations (Klypin et al., 1999); the "core-cusp halo problem", where observations of flat central dark matter distributions stand at odds with simulated predictions of cuspy density profiles (Moore,

1994); and the "too big to fail problem", which arises from the fact that simulations suggest that luminous satellites of the Milky Way should be much denser than we observe (Boylan-Kolchin et al., 2011). Some of these tensions may be resolvable through detailed observations of isolated LSBGs/UDGs, whose development have not been influenced by tidal forces and whose dark matter halos have been largely unperturbed by their baryonic matter content due to the fact that they are dark matter-dominated. Once again, this presents the need to have a large, representative sample of these objects, one which we will hopefully develop in the coming decades.

Because many of the values to be calculated herein depend on the cosmological model used, I will be adopting a standard flat ΛCDM model with $H_0 = 70$ km sec^{-1} Mpc^{-1}, $\Omega_m = 0.3$, and $\Omega_\Lambda = 0.7$. Additionally, all presented magnitudes use the AB system (Oke & Gunn, 1983), and have been corrected for galactic extinction using the dust maps of Schlegel et al. (1998), recalibrated in Schlafly & Finkbeiner (2011).

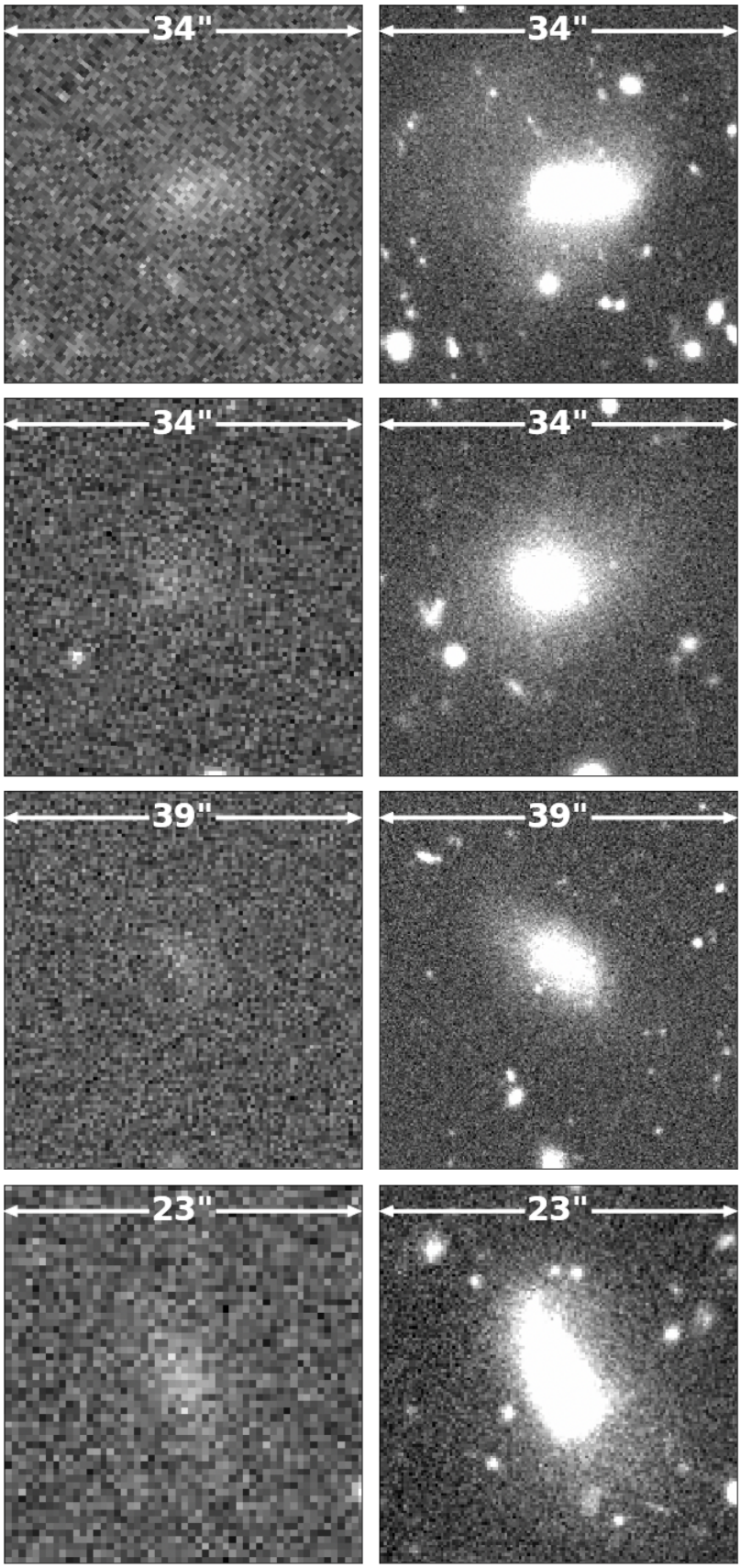

Figure 1.1 The four UDG candidates to be discussed herein. Each row is an i-band image of one of the objects as seen in SDSS (left) and as seen in HSC-SSP (right). Two of HSC-SSP's advantages over SDSS for low surface brightness studies are obvious: a lower surface brightness limit and a higher resolution.

Chapter 2

UDG Candidate Characterization

2.1 Sample Selection

Three of the four objects discussed in this thesis were originally identified as UDG candidates in Greco et al. (2018). This catalogue of 781 LSBGs was obtained from the first ~ 200 deg^2 of the Wide layer of HSC-SSP, an ongoing wide-field imaging survey using the Hyper Suprime-Cam (Miyazaki et al., 2018) at the Subaru Telescope. When completed, the Wide layer will cover ~ 1400 deg^2 of the sky to an i-band depth of ~ 26 mag (Aihara et al., 2018). These three were chosen for spectral analysis due to their being red ($g - i \geq 0.64$), potentially physically large ($r_{eff} > 2.5$ arcsec), and likely isolated ($r_{proj} > 400$ kpc projected distance from known galaxies of mass $M_* > 2.5 \times 10^{10} M_\odot$). The fourth object was discovered serendipitously when preparing for the observation runs. It was too blue and too bright to survive the initial cuts, but was close enough (~ 2.25 arcmin) to another target to allow for simultaneous observation of the two. An overview of the candidates is presented in Figure 2.1.

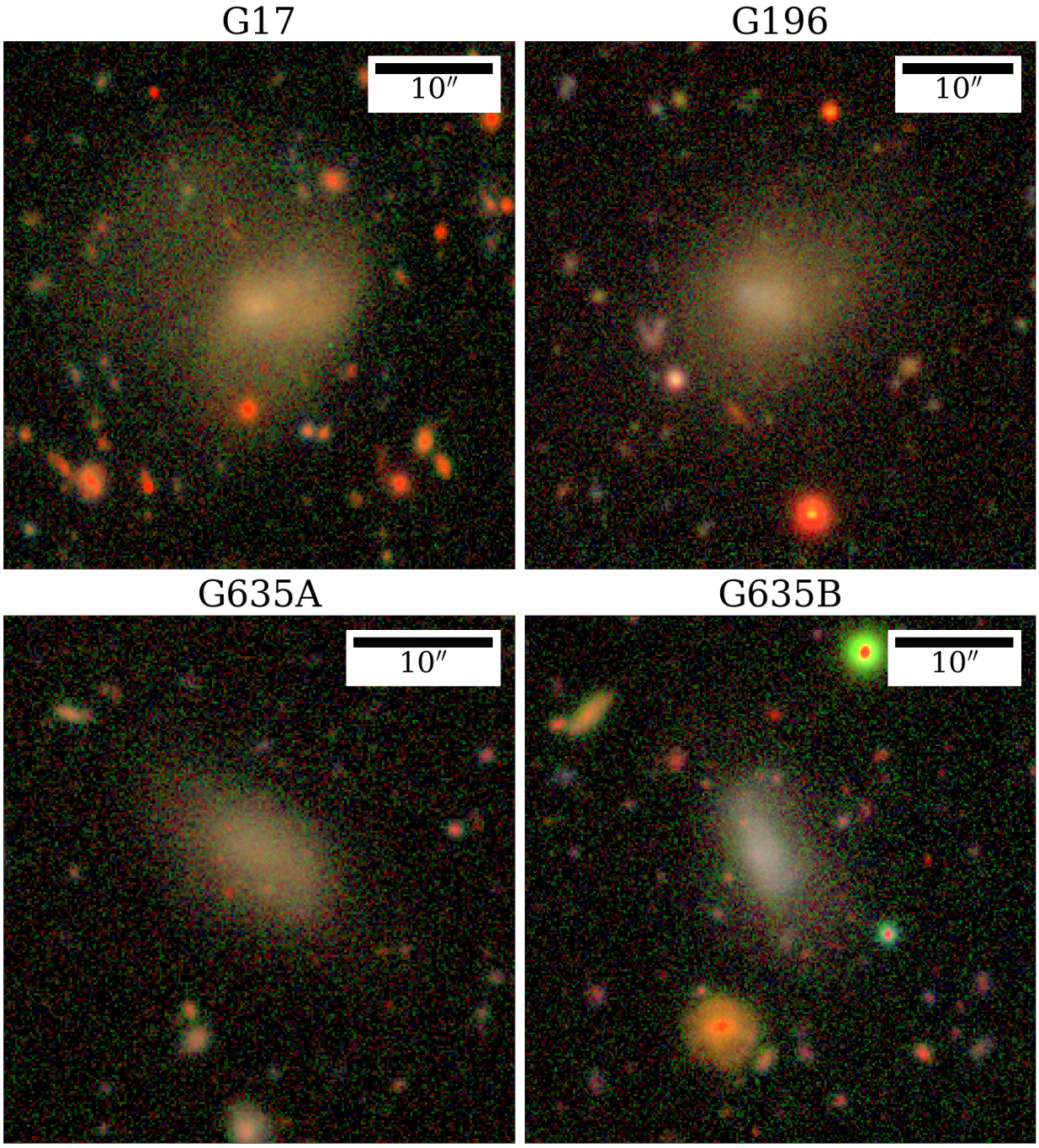

Figure 2.1 HSC-SSP *gri* composite images (Lupton et al., 2004) of the four UDG candidates under examination.

2.2 Redshift Identification

Spectra of these objects were obtained using the Multi-Object Double Spectrograph (MODS) (Pogge et al., 2010) onboard the Large Binocular Telescope (LBT) . MODS provides spectral coverage between 320 - 1050 nm, with a small coverage gap between 560 - 570 nm when operating in dual-channel mode. A 2.4 arcsec wide long slit was used to collect as much light as possible across the faces of these diffuse objects, at the expense of spectral resolution. Individual observations of each object were taken over the course of several months: September 16, 2018 (G196); March 29, 2019 (G17); and April 2, 2019 (G635A/B). For each object, three 1800 second exposures were obtained simultaneously in the red and blue channels for a total exposure time of 90 minutes. In all cases, seeing averaged around $\sim 1.0 \pm 0.2$ arcsec.

The raw spectra were reduced using a two-step process following the standard MODS reduction procedures. First, the spectra were run through the modsCCDRed program (Pogge, 2019), which median combined the exposures to eliminate transient events such as cosmic ray strikes on the detector, removed known bad pixel columns, and bias corrected the combined data. The ultimate output of this program was a color-free normalized pixel flat field image. These images were then fed through the modsIDL program (Croxall & Pogge, 2019), which performed sky subtraction; flux calibration using spectro-photometric standard stars; wavelength calibration using the spectra of Ne, Ar, Kr, Xe, and Hg lamps; and produced the final 2D and 1D spectra.

In general, redshifts can be measured either from absorption or emission lines. Emission line spectroscopy tends to be easier, but quenched galaxies are often lacking in emission features. For absorption line spectroscopy, we must resort to techniques such as cross-correlation, which Fourier transforms and convolves the spectrum of interest with a known spectrum to determine the most likely velocity shift between the two.

For these four objects, I first measured a redshift using the xcsao cross-correlation routine,

which is part of the RVSAO package for IRAF (Kurtz & Mink, 1998; Tody, 1986, 1993). To run cross-correlation, three stellar templates were used, representing samples of F-, K-, and A-type stars in M31. The results of these cross-correlations were then averaged together to arrive at the final redshifts. When possible, I confirmed these redshifts through emission spectroscopy by fitting a Gaussian to the features most likely be the [OII] 3726-3729Å doublet and the Hα 6562.8Å line. In all cases, the centroids of these lines were consistent with the cross-correlation redshifts. The spectrum of G196 is presented in Figure 2.2. The full sample of spectra is presented in Appendix A.

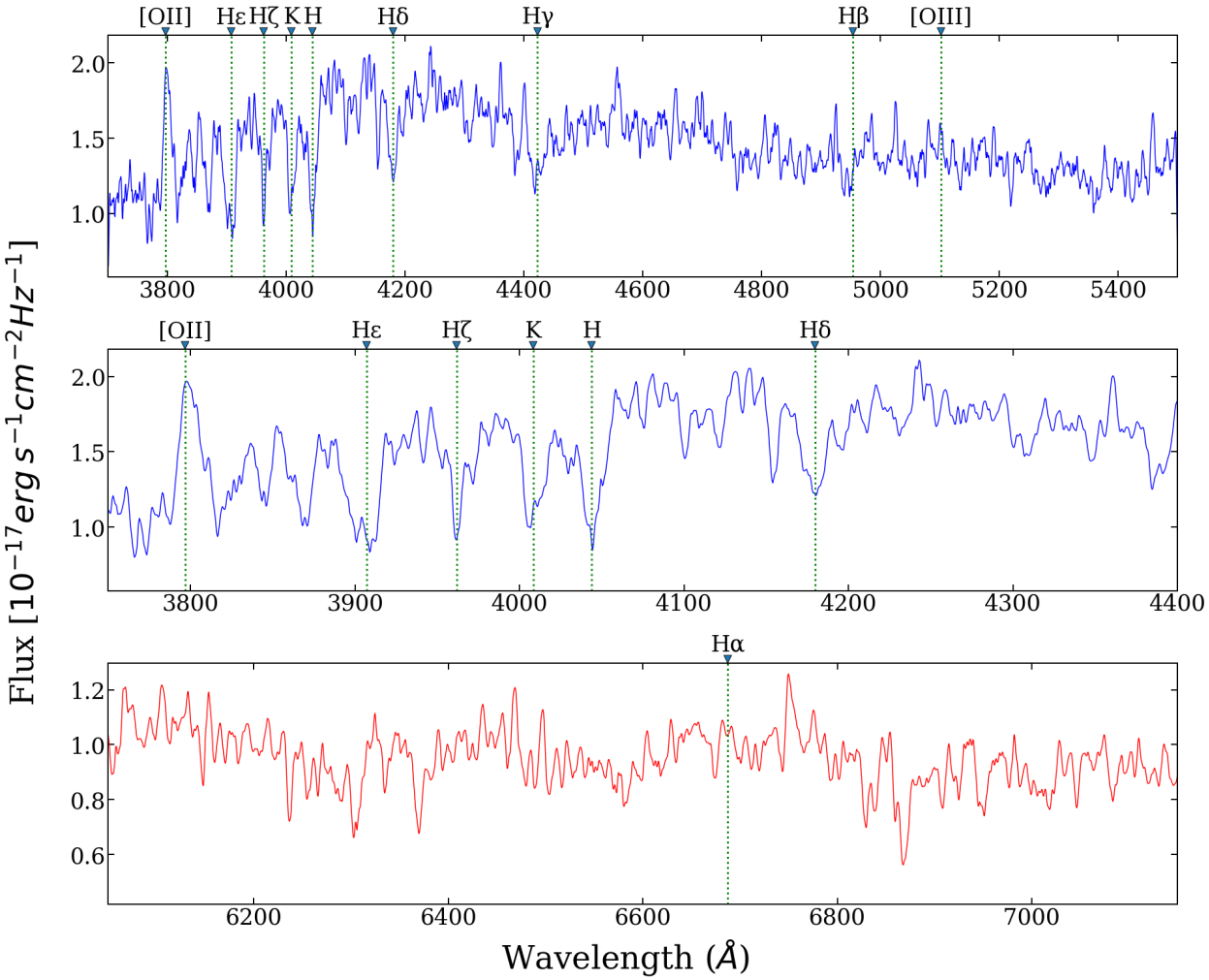

Figure 2.2 G196 spectrum. Of note here are the [OII] emission line and the Balmer absorption and H and K calcium absorption lines.

Interestingly, the spectra of these objects are quite dissimilar from each other. G17's

spectrum is characterized by very strong [OII] and Hα emission lines, and weak Hydrogen Balmer absorption lines. G196's spectrum shows a middling [OII] emission and Balmer absorption lines, but no Hα detection. G635A's spectrum is fairly chaotic, with no convincing [OII] or Balmer lines, but a weak Hα absorption feature. G635B displays very strong Balmer absorption lines, in addition to [OII] and Hα emission.

2.3 Physical Properties

Useful features of these objects to know include their distances and physical sizes, as well as their masses and luminosities. The concept of "distance" in cosmology can be surprisingly difficult to understand, due to the fact that the expanding universe is constantly changing the separation between objects and the fact that as we observe more distant objects, we are also looking back in time. Thankfully, there are a number of existing distance measurements, which are succinctly described in Hogg (1999). In brief, the traditional concept of distance (i.e. what you would measure with a ruler between two objects at the same point in time) is known as the *line-of-sight comoving distance*. In our assumed flat ΛCDM model, it is defined as:

$$D_c = D_H \int_0^z \frac{dz'}{E(z')} \tag{2.1}$$

Where $E(z') = \sqrt{\Omega_m(1+z')^3 + \Omega_\Lambda}$ and D_H is the Hubble distance $D_H = c/H_0$. To convert our angular effective radii into physical effective radii, we can use the *angular diameter distance*, the ratio of the object's physical size to its angular size. It is simply related to the comoving distance:

$$D_A = \frac{D_c}{1+z} \tag{2.2}$$

The luminosity can be obtained using the *luminosity distance*, which takes the place of the ordinary distance in the conversion between apparent and absolute magnitude:

$$M = m - 5(\log_{10}(D_L) - 1) \tag{2.3}$$

The luminosity distance can be calculated from the comoving and angular diameter distances:

$$D_L = (1+z)D_C \tag{2.4}$$

$$D_L = (1+z)^2 D_A \tag{2.5}$$

To get an estimate of the stellar mass of each of these objects, I used the relation given in Bell et al. (2003) that transforms a galaxy's color index to its mass-to-light ratio. The basic form of this equation is given in Equation 2.6.

$$\log_{10}\left(\frac{M}{L}\right) = a_\lambda + (b_\lambda \times \text{color}) \tag{2.6}$$

Where a_λ and b_λ are specific constants given for each color index and photometric color band. In this case, since these objects were selected by their $g-i$ color index, these constants take on the values $a_\lambda = -0.152$ and $b_\lambda = 0.518$. Use of this relation to estimate a stellar mass is possible because we know the distance to each object, and thus its luminosity.

For G17, G196, and G635A, I used the values for r_{eff}, $g-i$, and the i-band apparent magnitude published in Greco et al. (2018). However, since G635B was not included as part of this original discovery paper, I derived these values myself following the same methodology. To begin, unrelated bright objects were masked with an automatically generated object mask produced by *sep* (Barbary, 2016; Bertin & Arnouts, 1996). Then, G635B was modeled as a two-dimensional Sérsic function, convolved with the HSC PSF and variance images. The model was first generated with all free parameters in the i-band, then was refit in the g- and r- bands with all parameters other than the amplitude fixed at the i-band values.

Summary results of measured and derived properties are presented in Tables 2.1 and 2.2, respectively.

The placement of these objects in the wider context is presented in Figure 2.3. Alongside our objects are data on UDGs in medium- to high-density environments from van Dokkum et al. (2015) and Román & Trujillo (2017a), field UDGs with HI detections (Leisman et al.,

Table 2.1. Measured properties.

	G17	G196	G635A	G635B
RA	16:24:57.7	02:31:54.4	11:42:05.9	11:41:58.2
Dec	+43:03:31.9	-02:47:24.8	+00:21:09.9	+00:19:56.6
z	0.0583 ± 0.0002	0.0187 ± 0.0002	0.0178 ± 0.0003	0.0186 ± 0.0003
r_{eff} [arcsec]	6.10 ± 0.79	6.58 ± 0.79	4.68 ± 0.79	4.21 ± 0.79
m_i	18.18 ± 0.24	18.20 ± 0.24	19.31 ± 0.24	18.39 ± 0.24
g-r	0.57	0.50	0.44	0.19
g-i	0.87	0.76	0.66	0.27

Table 2.2. Derived properties.

	G17	G196	G635A	G635B
Distance [Mpc]	246.4 ± 0.8	79.7 ± 0.8	75.9 ± 1.3	79.3 ± 1.3
r_{eff} [kpc]	6.9 ± 1.1	2.5 ± 0.3	1.7 ± 0.3	1.6 ± 0.3
M_i	-18.90 ± 0.77	-16.35 ± 0.22	-15.12 ± 0.19	-15.57 ± 0.47
M_* $[10^8 M_\odot]$	46.9 ± 12.0	3.92 ± 1.08	1.13 ± 0.33	1.81 ± 0.53

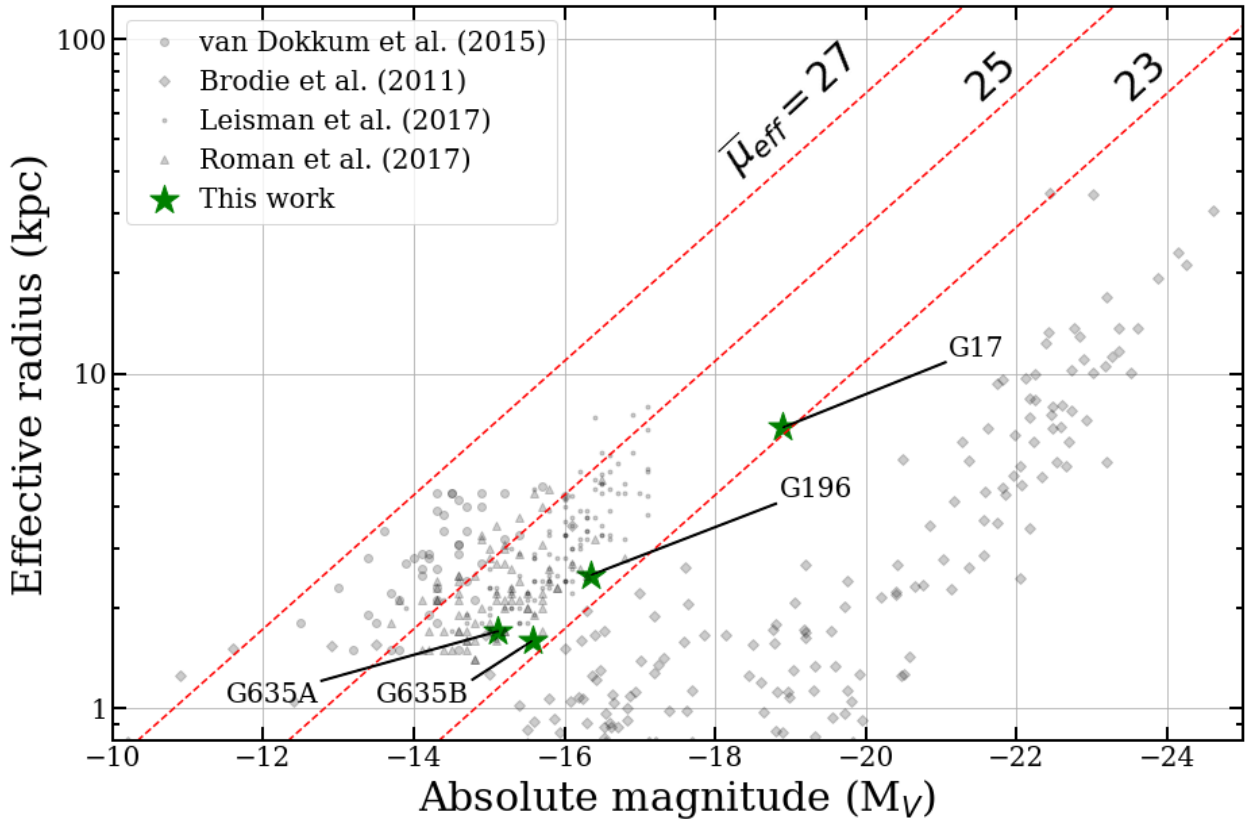

Figure 2.3 Comparison of our UDG candidates with other known UDGs and early-type galaxies. G17 clearly stands out as an unusual object in this sample. The others are consistent with the size one would expect from UDGs, though they are somewhat too luminous.

2017), and a selection of early-type galaxies (Brodie et al., 2011). G196, G635A, and G635B all sit relatively close to the UDG magnitude-radius regime described in van Dokkum et al. (2015), though their surface brightnesses are somewhat brighter than the typical UDG. G17, on the other hand, appears to be a much more unusual object. Its unexpectedly high redshift resulted in a size and absolute magnitude that are both much too large for this to be considered a "traditional" UDG. Both are more similar to a galaxy like M33 than to any of the other objects presented here.

An important consideration to keep in mind is that these redshifts are not a definitive measure of these objects' distances. In converting a redshift to a distance, one assumes that the measured velocity is solely the recessional velocity caused by the expansion of the universe. However, this is not strictly true. They each have a peculiar velocity, i.e. their

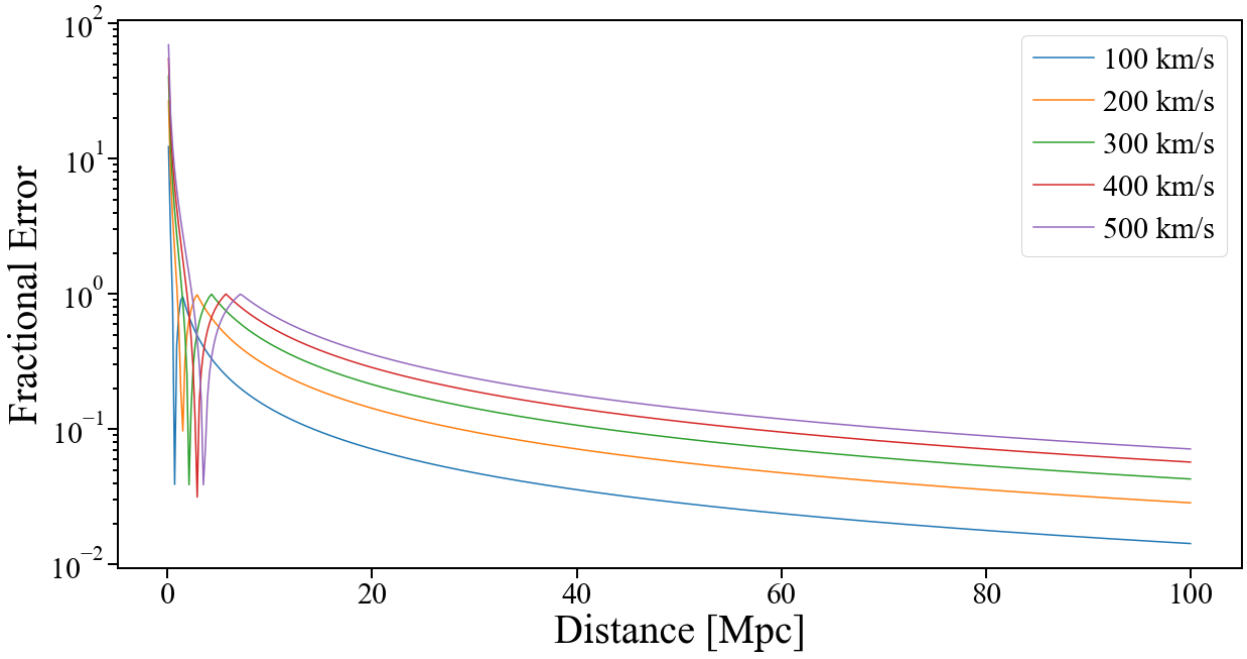

Figure 2.4 Fractional errors in a velocity measurement due to various values of the peculiar velocity. Beyond distances of $\sim$ 60 kpc or so, the error is on the order of $\sim$ 10% for all but the largest peculiar velocities. For the typical redshifts we measure here, a 10% error in the velocity measurement would introduce an uncertainty of $\sim \pm 0.002$ into the redshift measurement.

velocity relative to the average expansion rate of the universe, as well. If a significant portion of that peculiar velocity is along the line of sight, then it can have a significant effect on the redshift. If the radial component of the peculiar velocity is towards us, it will reduce the redshift and result in a closer distance measurement, and vice versa. Fortunately, this is only a serious problem for nearby galaxies. Beyond this, the Hubble flow dominates velocity measurements, allowing us to safely ignore peculiar velocity concerns. This effect can be seen in Figure 2.4, which shows the fractional error in a velocity measurement due to peculiar velocities of $100 - 500$ km sec^{-1}. These errors were calculated using the Hubble flow velocity at a given distance as the true velocity value, then subtracting the peculiar velocity from that to use as the measured velocity value.

Chapter 3

Environments

With redshifts in hand, it is now possible to determine where these objects lie in relation to other galaxies through comparisons with well-established catalogues. In this case, this comparison was done with version v101 of the NASA-Sloan Atlas (NSA), which contains information on nearly every galaxy with a known redshift out to $z = 0.15$ within the coverage of SDSS DR8. The NSA masses are given in units of $M_{\odot}h^{-2}$. The masses presented here were calculated with $h = 0.7$, in keeping with the standard cosmological model adopted throughout this work.

I searched the NSA to identify any objects of mass $> 10^9 M_{\odot}$ with a projected distance within 500 kpc and a measured velocity within 500 km sec^{-1} of each of the four targets. This mass cutoff was chosen to be slightly lower than the initial targeting parameters described in Chapter 2 to see if these objects might be associated with lower-mass galaxies. The velocity difference was chosen as the range at which one could make a plausible argument for physical association, rather than line-of-sight projection effects.

A chart of the environment around G196 is presented in Figure 3.1, and the full sample of environments can be found in Appendix B. Details on each of the surrounding galaxies are presented in Table 3.

Each of these objects is relatively close to at least one intermediate-size galaxy. In the case of G196 and G635A, the potential hosts were just outside of the initial cutoffs. While

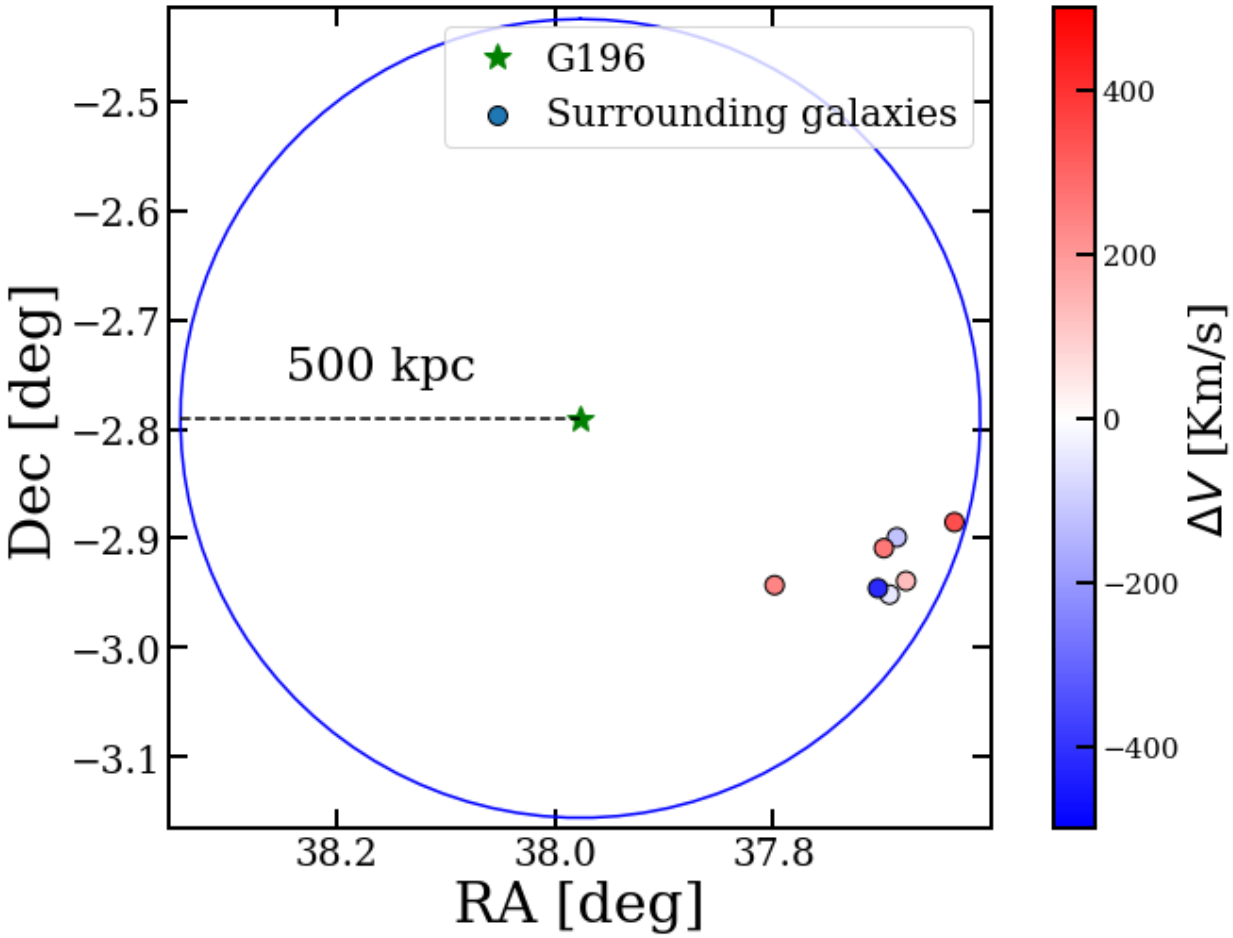

Figure 3.1 G196 appears to be near the very edge of a small group of galaxies that is anchored by NGC 958, with an SDSS-estimated stellar mass of 1.93×10^{11} $M_{\odot}$. This is the most massive of the hosts found in this work.

the mass of G196's host ($\sim 10^{11} M_{\odot}$) was significantly above the cutoff ($2.5 \times 10^{10} M_{\odot}$), its projected separation ($\sim$ 455 kpc) is just outside the cutoff limit of 400 kpc. Similarly, while G635A's host is well within the separation cutoff, its mass is just below the "massive" cutoff. In the case of G17, the fact that its hosts' stellar masses and projected separations should have eliminated it from the initial sample, its comparatively high redshift meant that these hosts were not present in the version of the NSA used in Greco et al. (2018) (v012), which only covered galaxies out to $z \sim 0.05$.

The fact that these objects are not completely isolated, particularly the fact that they appear to be physically associated with the closest large galaxy in projected separation, also

Table 3.1. Galaxies at close projected separation to each of the four targets.

Object Name	Nearby Galaxy Name	Nearby Galaxy Stellar Mass [$M_\odot$]	Velocity Difference [km/s]	Projected Separation [kpc]
G17				
	J162501.31+430233.7	5.05×10^{10}	-136.63	78.40
G196				
	J023032.19-025303.0	4.54×10^{9}	344.13	485.17
	NGC 958	1.93×10^{11}	131.98	454.99
	J023044.79-025356.9	4.37×10^{9}	-118.19	422.56
	J023046.40-025705.0	6.77×10^{9}	-45.14	444.76
	J023047.70-025430.9	2.09×10^{9}	264.07	412.57
	J023048.99-025645.0	1.45×10^{9}	-417.40	428.32
	J023111.59-025634.0	1.75×10^{10}	241.06	320.09
G635A				
	J114212.25+002004.0	1.32×10^{10}	226.29	41.84
	G635B	1.81×10^{8}	240.00	49.05

gives us additional confidence in our redshift measurements. As mentioned in Chapter 2, a relatively small peculiar velocity can have a similarly small (but still significant) effect on the redshift measurement. If this effect was non-negligible, it would be an astonishing coincidence for these UDG candidates to have measured redshifts near those of their closest neighbors on the sky. It is far more likely that the measured redshifts are extremely close to the actual redshifts, i.e. that their peculiar velocities along the line of sight are small.

Chapter 4

Conclusions and Future Work

In this thesis, I have presented spectroscopic confirmation and associated physical properties of four ultra diffuse galaxy candidates initially identified in the Wide layer of HSC-SSP. Three of the four (G196, G635A, and G635B) are roughly consistent with UDGs that have been previously identified, with $r_{eff} \sim 1.5 - 2.5$ kpc and estimated stellar masses of $\sim 10^8 M_{\odot}$. While their mean effective surface brightnesses of $\sim 23 - 24$ mag arcsec^{-2} are slightly above the common cutoff of ~ 24 mag arcsec^{-2} g-band central surface brightness usually used to define UDGs, previous studies of similar objects (e.g. Trujillo et al., 2017; Román & Trujillo, 2017b) have demonstrated that passive stellar evolution will bring their surface brightnesses safely within the UDG range in < 10 Gyrs.

With the exception of G635A, all of the targets displayed relatively strong [OII] emission features, with G17 and G635B also displaying a strong Hα emission line. The presence of these emission lines has allowed for increased confidence in the redshift measurements, as they can be used to confirm cross-correlation estimates. Additionally, the strength of G635B's Balmer absorption lines suggests that it may be a post-starburst galaxy, which is consistent with its bluer color.

Even though all of these UDG candidates were originally selected due to being potentially isolated, none of them truly are. All of them appear to be physically associated with the nearest (in projected distance) large galaxy, though they are projected to be in the outskirts

of their respective host's virial radius. This is further evidence against the existence of red UDGs in the field and is consistent with theories that UDGs are quenched through environmental interactions, though we should not that our sample is very incomplete. However, we emphasize that the environments in which these UDGs reside is unlike those in which the majority of UDGs with confirmed redshifts discovered to date have been found. Instead of existing in the field or in a large galaxy cluster, these UDGs are associated with a small (< 10) number of small- to intermediate-sized ($10^9 - 10^{11} M_\odot$) galaxies. This suggests that they represent an interesting transitional regime worth further investigation.

These results illustrate the immense power of HSC-SSP and similar surveys in uncovering the mysteries of the low surface brightness universe. Even with just these four objects, it could be illuminating to more closely examine their dynamics. G17, for example, is significantly larger than the others and appears to have some tidal debris along its northern edge. This may be linked to its association with a triplet of merging galaxies. The G635 system is also quite intriguing, as the two UDGs are significantly different in color and in their spectra, despite being roughly the same size, the same shape, and at approximately the same distance from their host, which itself shows signs of significant tidal disruptions. By continuing to study these objects, we can extend our understanding of the mechanisms behind galaxy formation, stellar feedback, the properties of dark matter halos, and, ultimately, rigorously test the accuracy of the ΛCDM cosmological model.

Appendix A

Spectra

This appendix presents the measured spectra for each of the objects. Each consists of three panels. The upper panel is the blue (3900 - 5500 Å) part of the spectrum and the lower panel is the red (6000 - 7200 Å) part. The middle panel is a zoom-in on the part of the blue spectrum with the highest line density (3750 - 4400 Å) for the sake of clarity.

One should also note that the spectral line locations given in each plot do not necessarily imply that that line was actually identified. They are simply representative, showing where each line would be at the measured redshift.

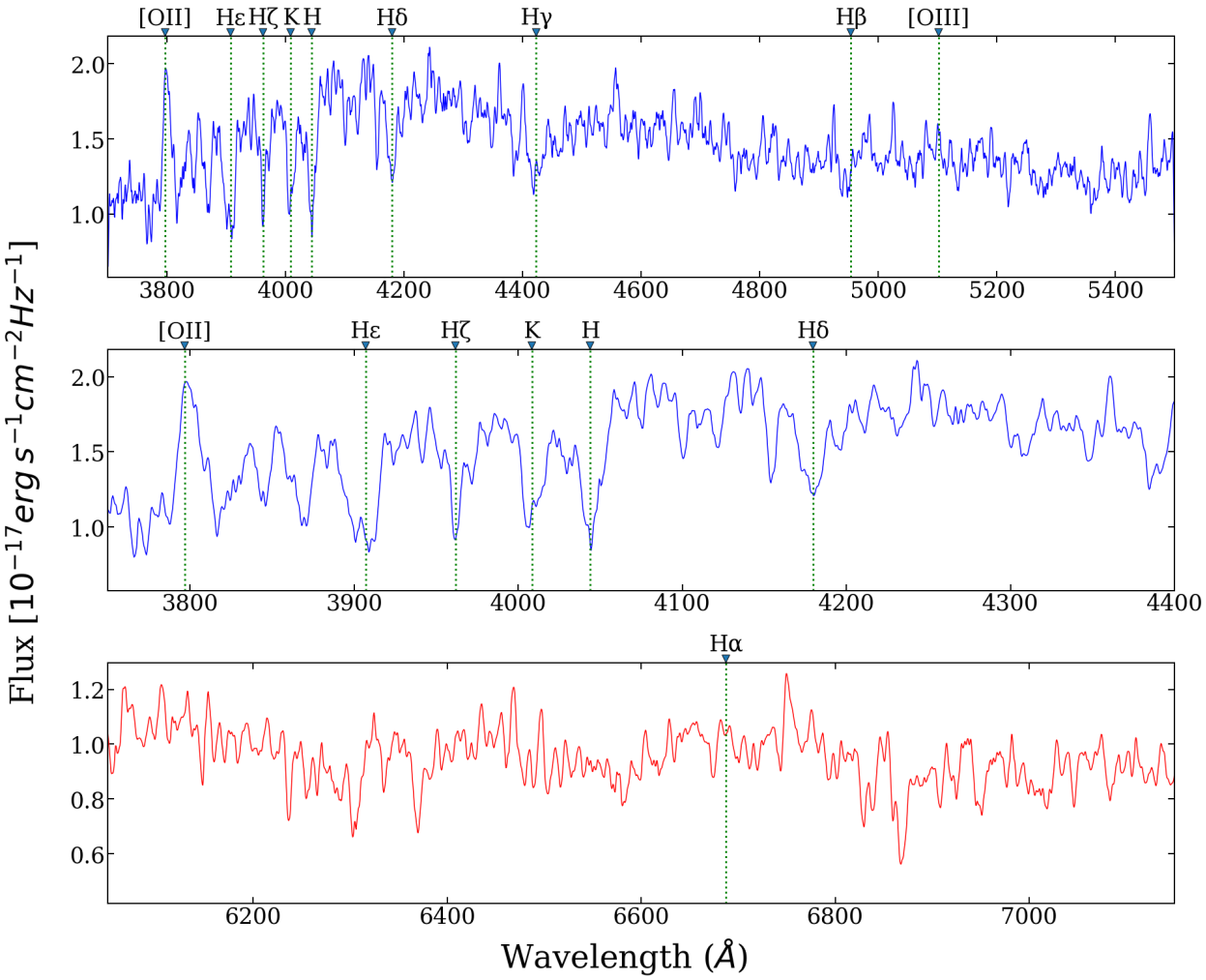

Figure A.1 G196 spectrum. Of note here are the [OII] emission line and the Balmer absorption and H and K calcium absorption lines.

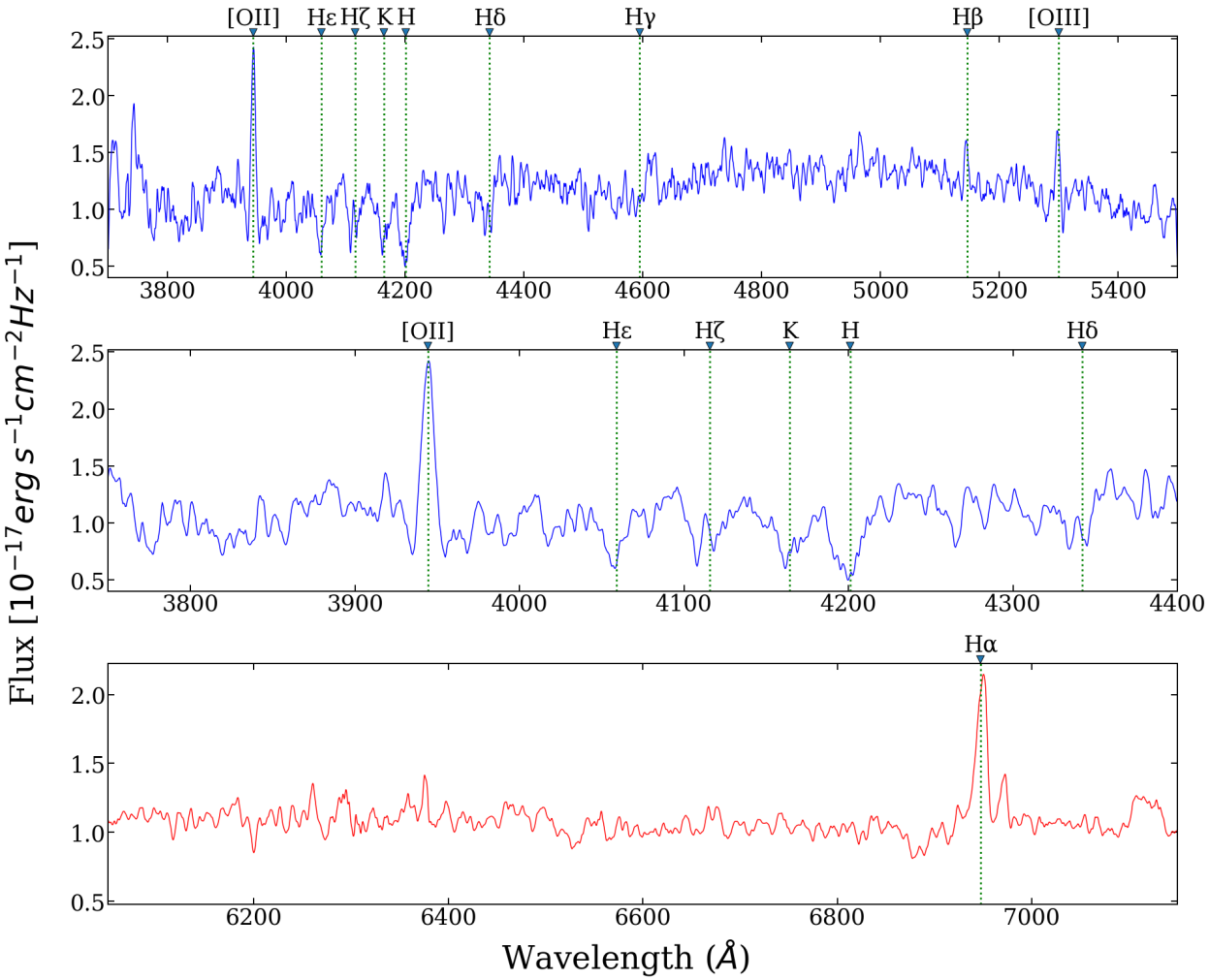

Figure A.2 G17 spectrum. This spectrum has extremely strong [OII] and Hα emission detections, as well as possible [OIII] and Hβ emission detections. The Balmer absorption lines are comparatively weak.

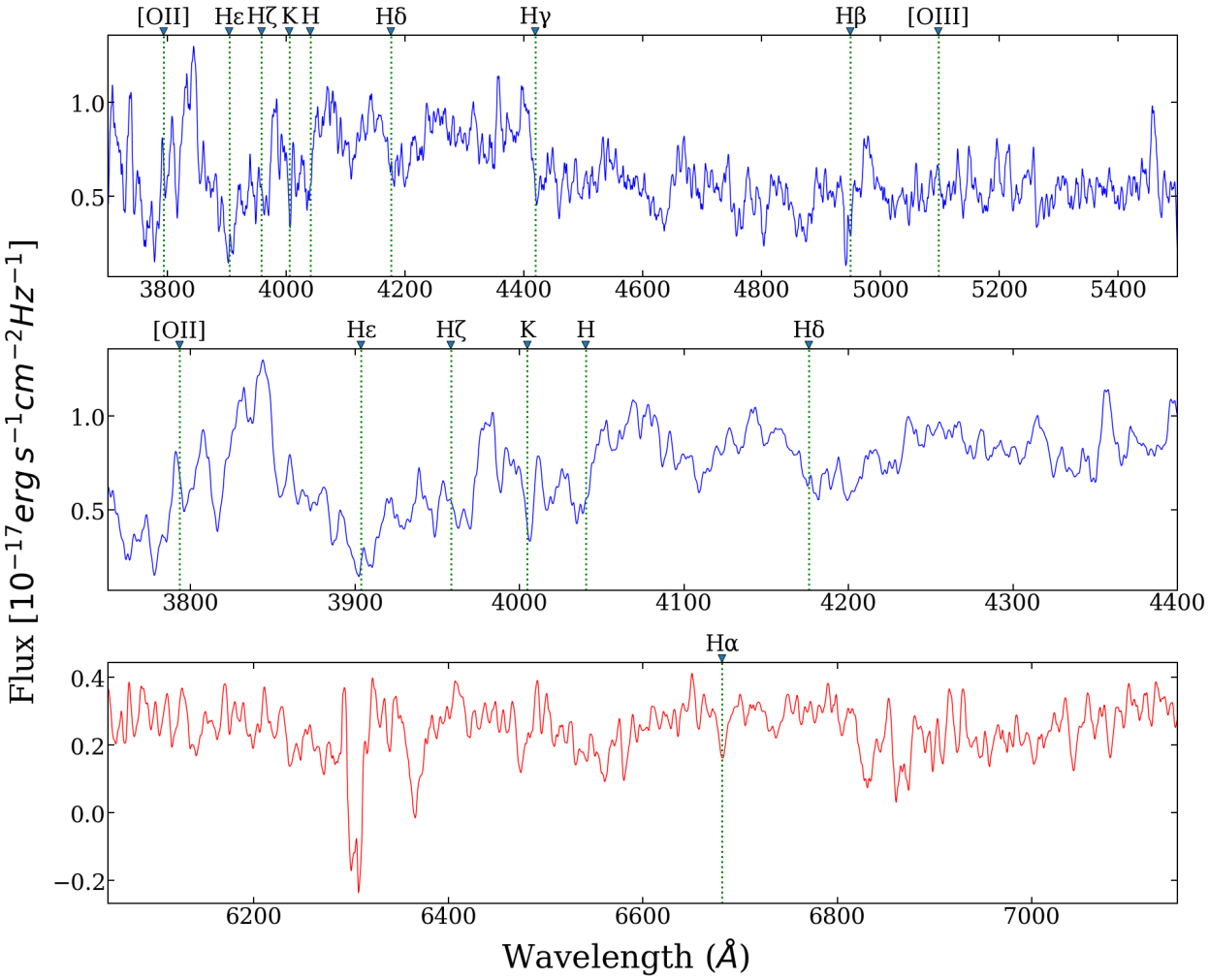

Figure A.3 G635A spectrum. Line detections here are very weak. There are no noticeable emission features, but there may be an Hα absorption feature.

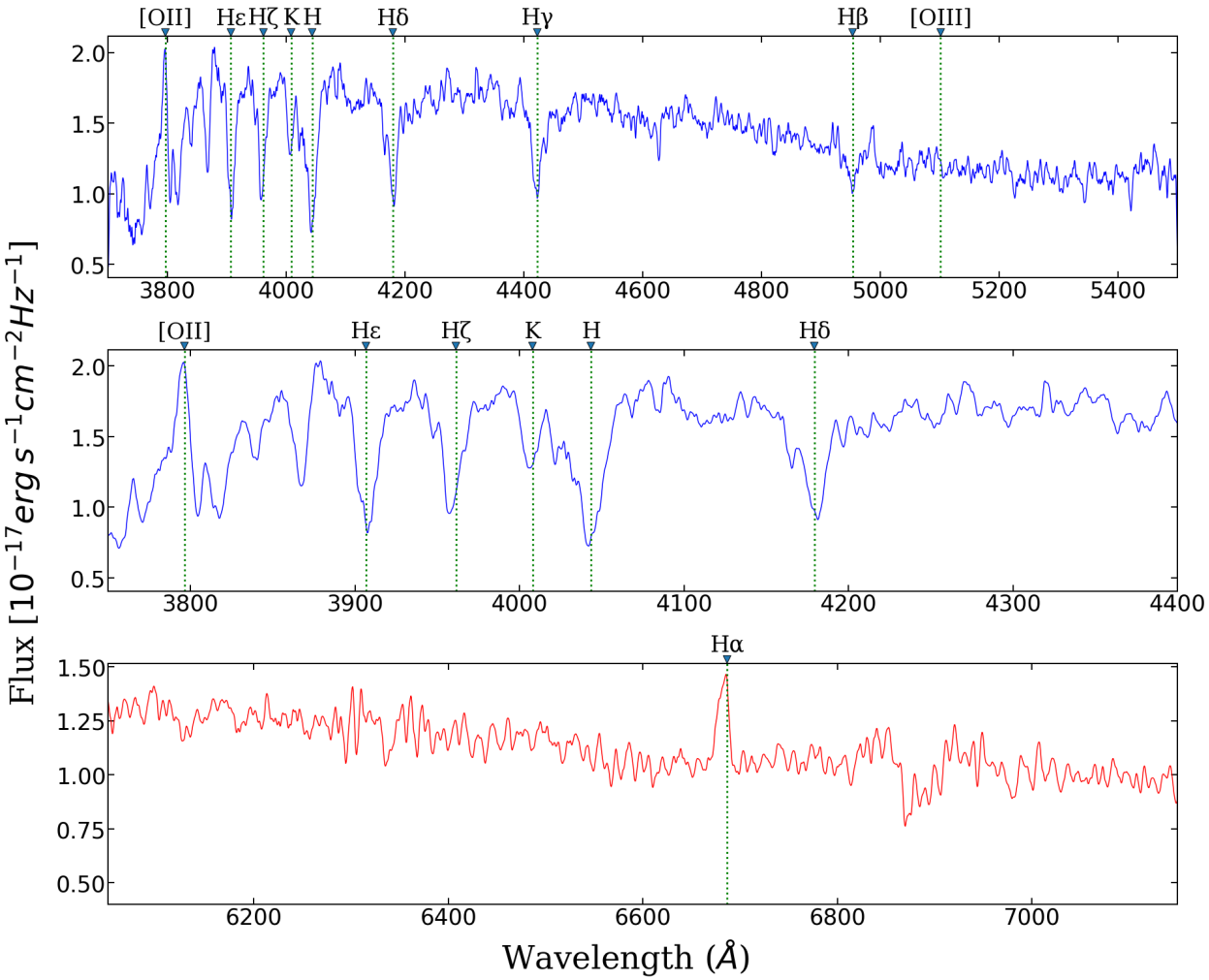

Figure A.4 G635B spectrum. This is a very vigorous spectrum, with robust [OII] and Hα emission detections as well as very strong Balmer absorption features, consistent with what would be expected of a post-starburst galaxy.

Appendix B

Environments

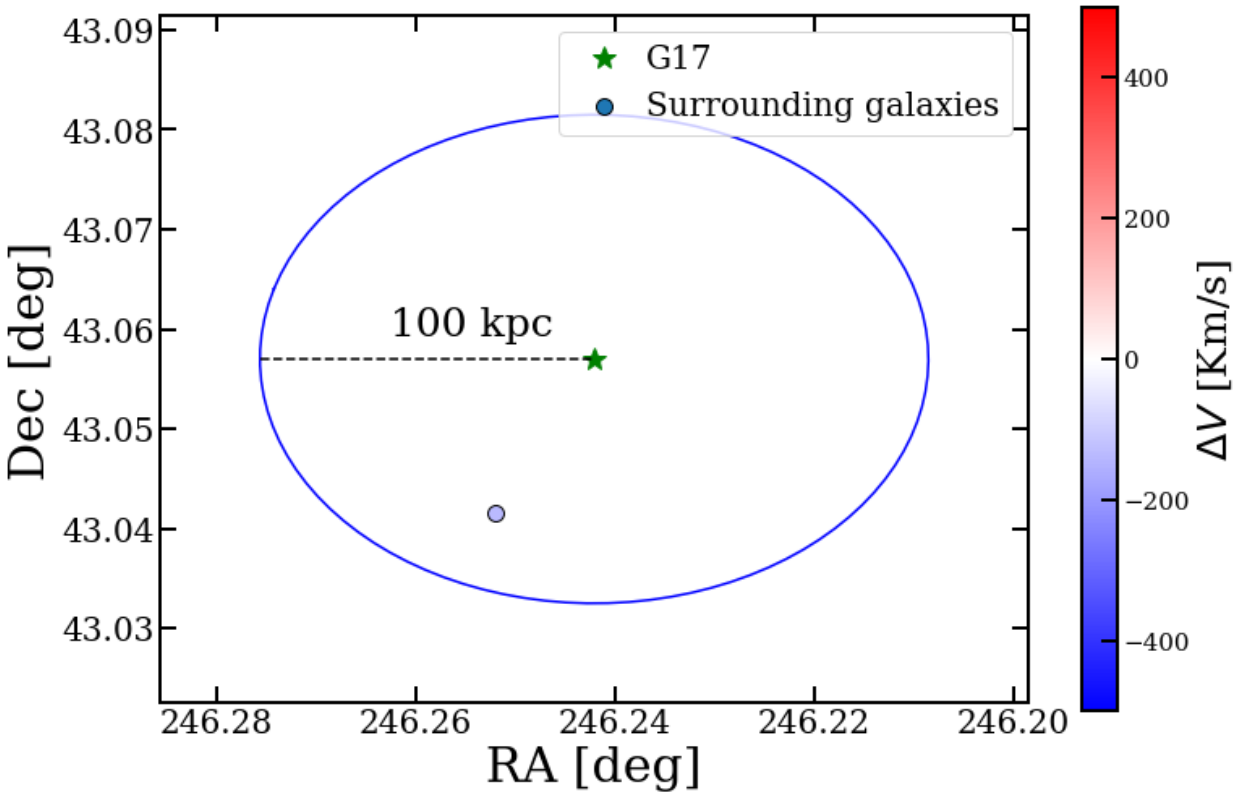

Figure B.1 G17 and nearby galaxies. At this relatively high declination, the 100 kpc equidistant circle becomes distorted by the projection. There was only one nearby galaxy found in the NSA catalogue though there are three near the marked position, as can be seen in Fig. B.6.

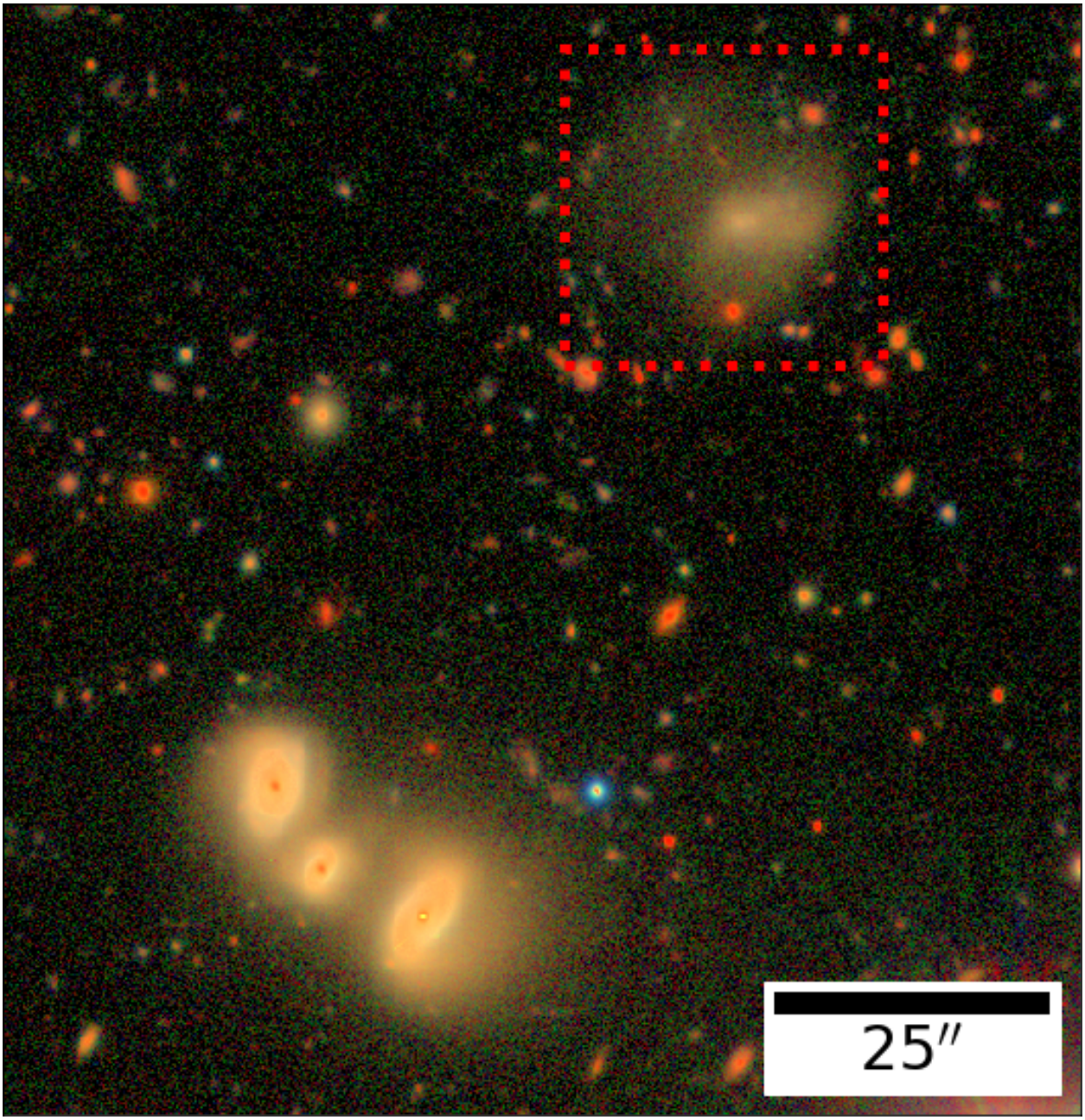

Figure B.2 HSC-SSP *gri* composite image of the environment around G17 (boxed). Of the trio of galaxies in the lower left, only one was catalogued in the NSA, though all are likely associated.

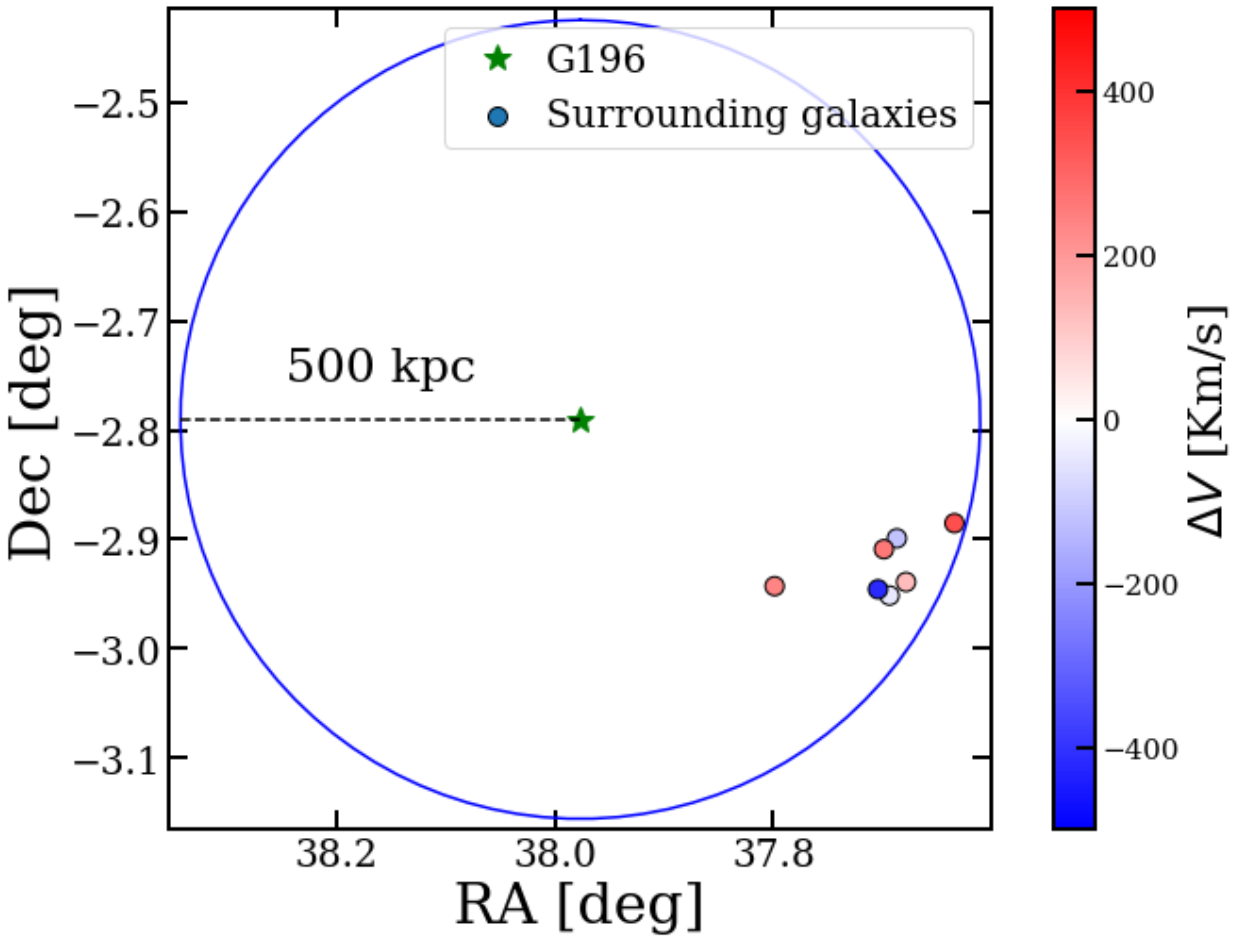

Figure B.3 G196 appears to be near the very edge of a small group of galaxies that is anchored by NGC 958, with an SDSS-estimated stellar mass of 1.93×10^{11} $M_{\odot}$. This is the most massive of the hosts found in this work.

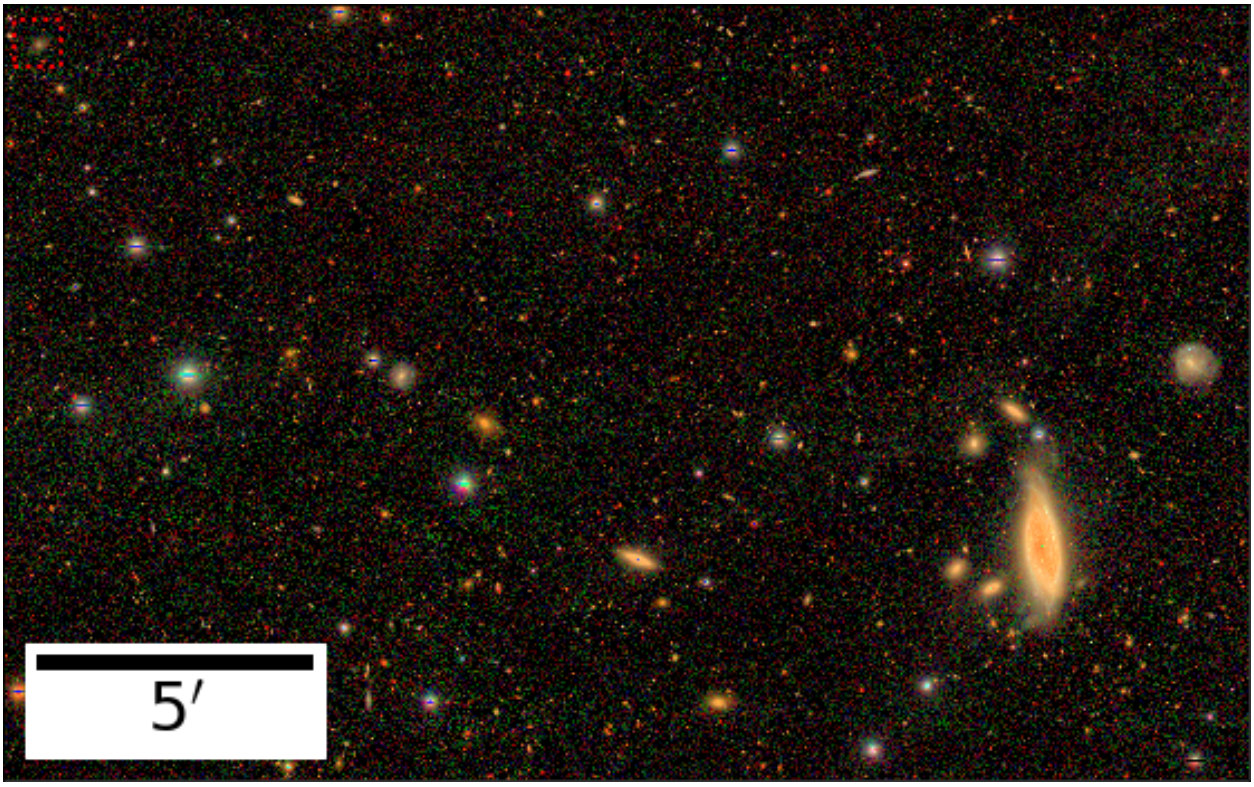

Figure B.4 HSC-SSP *gri* composite image of the environment around G196 (boxed, upper left).

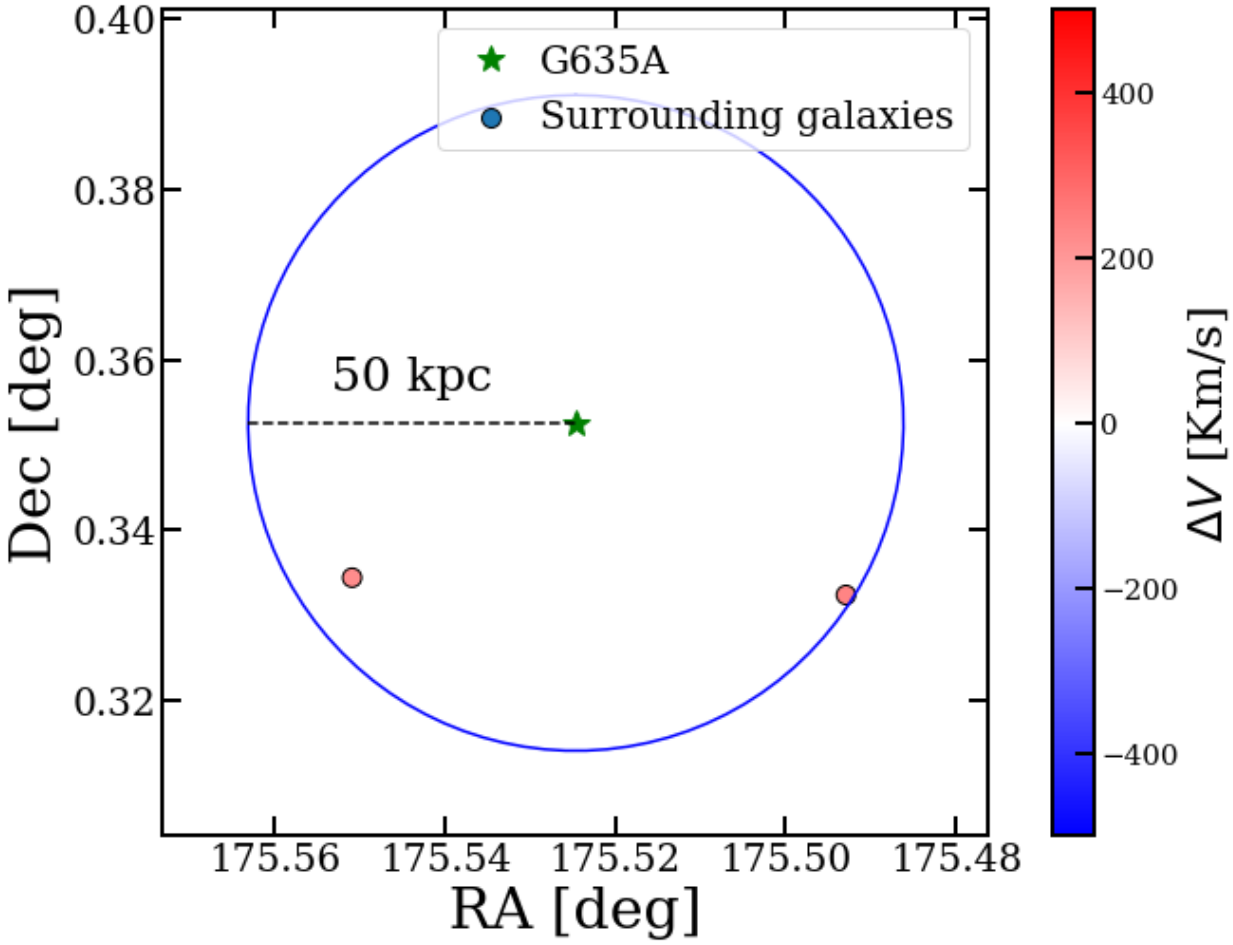

Figure B.5 G635A and nearby galaxies. Note that the object in the lower right is G635B, which had to be manually added as it was not included in any of the catalogs.

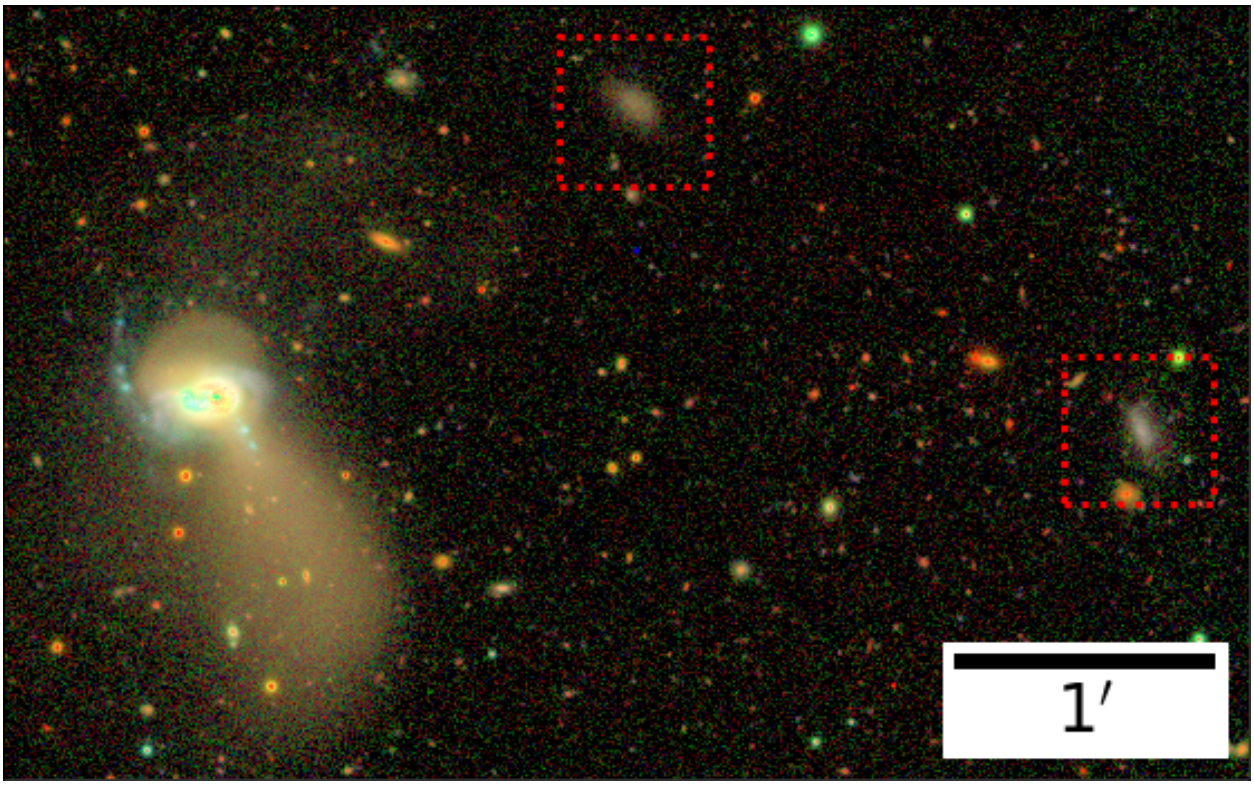

Figure B.6 HSC-SSP *gri* composite image of the environment around G635A (boxed, upper center) and G635B (boxed, lower right).

References

Abraham, R. G., & van Dokkum, P. G. 2014, PASP, 126, 55, doi: 10.1086/674875

Aihara, H., Arimoto, N., Armstrong, R., et al. 2018, PASJ, 70, S4, doi: 10.1093/pasj/psx066

Amorisco, N. C., & Loeb, A. 2016, MNRAS, 459, L51, doi: 10.1093/mnrasl/slw055

Barbary, K. 2016, Journal of Open Source Software, 1, 58, doi: 10.21105/joss.00058

Bell, E. F., McIntosh, D. H., Katz, N., & Weinberg, M. D. 2003, ApJS, 149, 289, doi: 10.1086/378847

Bertin, E., & Arnouts, S. 1996, A&AS, 117, 393, doi: 10.1051/aas:1996164

Boylan-Kolchin, M., Bullock, J. S., & Kaplinghat, M. 2011, MNRAS, 415, L40, doi: 10.1111/j.1745-3933.2011.01074.x

Brodie, J. P., Romanowsky, A. J., Strader, J., & Forbes, D. A. 2011, AJ, 142, 199, doi: 10.1088/0004-6256/142/6/199

Croxall, K. V., & Pogge, R. W. 2019, rwpogge/modsIDL: modsIDL Binocular Release, v1.0, Zenodo, doi: 10.5281/zenodo.2561424

Dalcanton, J. J., Spergel, D. N., Gunn, J. E., Schmidt, M., & Schneider, D. P. 1997a, AJ, 114, 635, doi: 10.1086/118499

Dalcanton, J. J., Spergel, D. N., & Summers, F. J. 1997b, ApJ, 482, 659, doi: 10.1086/304182

Dark Energy Survey Collaboration, Abbott, T., Abdalla, F. B., et al. 2016, MNRAS, 460, 1270, doi: 10.1093/mnras/stw641

de Jong, J. T. A., Verdoes Kleijn, G. A., Boxhoorn, D. R., et al. 2015, A&A, 582, A62, doi: 10.1051/0004-6361/201526601

Di Cintio, A., Brook, C. B., Dutton, A. A., et al. 2017, MNRAS, 466, L1, doi: 10.1093/mnrasl/slw210

Disney, M. J. 1976, Nature, 263, 573, doi: 10.1038/263573a0

El-Badry, K., Wetzel, A., Geha, M., et al. 2016, ApJ, 820, 131, doi: 10.3847/0004-637X/820/2/131

Freeman, K. C. 1970, ApJ, 160, 811, doi: 10.1086/150474

Geha, M., Blanton, M. R., Yan, R., & Tinker, J. L. 2012, ApJ, 757, 85, doi: 10.1088/0004-637X/757/1/85

Greco, J. P., Greene, J. E., Strauss, M. A., et al. 2018, ApJ, 857, 104, doi: 10.3847/1538-4357/aab842

Hogg, D. W. 1999, arXiv e-prints, astro. https://arxiv.org/abs/astro-ph/9905116

Impey, C., & Bothun, G. 1997, ARA&A, 35, 267, doi: 10.1146/annurev.astro.35.1.267

Ivezic, Z., Axelrod, T., Brandt, W. N., et al. 2008, Serbian Astronomical Journal, 176, 1, doi: 10.2298/SAJ0876001I

Klypin, A., Kravtsov, A. V., Valenzuela, O., & Prada, F. 1999, ApJ, 522, 82, doi: 10.1086/307643

Kurtz, M. J., & Mink, D. J. 1998, PASP, 110, 934, doi: 10.1086/316207

Leinert, C., Bowyer, S., Haikala, L. K., et al. 1998, A&AS, 127, 1, doi: 10.1051/aas:1998105

Leisman, L., Haynes, M. P., Janowiecki, S., et al. 2017, ApJ, 842, 133, doi: 10.3847/1538-4357/aa7575

Lupton, R., Blanton, M. R., Fekete, G., et al. 2004, PASP, 116, 133, doi: 10.1086/382245

McGaugh, S. S. 1994, ApJ, 426, 135, doi: 10.1086/174049

McGaugh, S. S., & Bothun, G. D. 1994, AJ, 107, 530, doi: 10.1086/116874

McGaugh, S. S., Schombert, J. M., & Bothun, G. D. 1995, AJ, 109, 2019, doi: 10.1086/117427

Miyazaki, S., Komiyama, Y., Kawanomoto, S., et al. 2018, PASJ, 70, S1, doi: 10.1093/pasj/psx063

Moore, B. 1994, Nature, 370, 629, doi: 10.1038/370629a0

Oke, J. B., & Gunn, J. E. 1983, ApJ, 266, 713, doi: 10.1086/160817

Pogge, R. 2019, rwpogge/modsCCDRed 2.0, 2.0, Zenodo, doi: 10.5281/zenodo.2550741

Pogge, R. W., Atwood, B., Brewer, D. F., et al. 2010, Society of Photo-Optical Instrumentation Engineers (SPIE) Conference Series, Vol. 7735, The multi-object double spectrographs for the Large Binocular Telescope, 77350A, doi: 10.1117/12.857215

Román, J., & Trujillo, I. 2017a, MNRAS, 468, 703, doi: 10.1093/mnras/stx438

—. 2017b, MNRAS, 468, 4039, doi: 10.1093/mnras/stx694

Sandage, A., & Binggeli, B. 1984, AJ, 89, 919, doi: 10.1086/113588

Schlafly, E. F., & Finkbeiner, D. P. 2011, ApJ, 737, 103, doi: 10.1088/0004-637X/737/2/103

Schlegel, D. J., Finkbeiner, D. P., & Davis, M. 1998, ApJ, 500, 525, doi: 10.1086/305772

Tody, D. 1986, Society of Photo-Optical Instrumentation Engineers (SPIE) Conference Series, Vol. 627, The IRAF Data Reduction and Analysis System, ed. D. L. Crawford, 733, doi: 10.1117/12.968154

—. 1993, Astronomical Society of the Pacific Conference Series, Vol. 52, IRAF in the Nineties, ed. R. J. Hanisch, R. J. V. Brissenden, & J. Barnes, 173

Trujillo, I., Roman, J., Filho, M., & Sánchez Almeida, J. 2017, ApJ, 836, 191, doi: 10.3847/1538-4357/aa5cbb

van Dokkum, P. G., Abraham, R., Merritt, A., et al. 2015, ApJL, 798, L45, doi: 10.1088/2041-8205/798/2/L45

York, D. G., Adelman, J., Anderson, John E., J., et al. 2000, AJ, 120, 1579, doi: 10.1086/301513